Stability analysis of a non-linear drill string with the axial-torsional coupled vibration influenced by a non-Newtonian mud rheology model

Kamal Aghadadi[a], Firooz Bakhtiari-Nejad[a], Afshin Taghvaeipour[a], Ali Hosseinzadeh[a], AD Shaw[b]*

[a] *Department of Mechanical Engineering, Amirkabir University of Technology, Iran*

[b] *Department of Aerospace Engineering, Swansea University, Swansea SA2 8PP, UK*

[*] *Corresponding author. Email:* afshin.taghvaeipour@gmail.com

Abstract

This paper aims to investigate the effect of drilling mud on the stability of nonlinear coupled axial-torsional motion of a drill string. Due to the development of high-performance computer systems, in this study, the behavior of mud is considered non-Newtonian and nonlinear, and the effect of drilling mud damping on both axial and torsional motion is simulated by means of the Herschel-Bulkley rheology model to present the more precise and intricate drilling string models. Due to the existence of delayed expressions in the state equations of the drilling system, a semi-discretization method is used to analyze the stability of drilling system. The result of stability analysis is then plotted on the plane of nominal rotational speed and weight on the bit (WOB). It is shown that the damping effect of drilling mud in the axial motion has no effect on the stability boundaries, while the influence on the torsional motion is significant. Thereafter, the effect of drilling mud parameters, such as fluid consistency index and power-law exponent, on system stability is investigated for the parameter range of experimental values. The results revealed that by increasing the fluid consistency index and power-law exponent, the stability zone is enlarged, and as a result, drilling operation at lower rotational speeds with higher WOB values can be feasible.

Keywords: drill string, drill mud, nonlinear dynamics, Herschel-Bulkley rheology, stability, delay differential equations

Nomenclature

Parameter	Definition	Unit
ρ	Density of drill string	kg/m^3
A	Cross -sectional area	m^2
J	Polar moment of inertia	m^4
D	Diameter of the drill string cross section	m
D_o	External diameters of the drill string cross section	m
D_i	Internal diameters of the drill string cross section	m
E	Young's modulus	Pa
G	Shear modulus	Pa
a	Drill bit radius	m
l	Drill bit wear-flat length	m
ε	Intrinsic specific energy related to the rock strength	Pa
γ	Drill bit geometry effect	--
μ	Friction coefficient	--
A_d	Contact surface between mud and drill string	m^2
Δ	Thickness of the mud layer	m
v	Mud flow rate	m^3/s

k_f	Consistency index	Pa.s^{n_f}
n_f	Power-law exponent	--
τ_{Hy}	Herschel-Bulkley yield stress	Pa
ω_d	Nominal rotary speed of the drill string	rad/s
L	Total length of the drill pipe	m
d_C	Cutting depth	m
M	Total mass of drill pipe	Kg
g	Acceleration of gravity	m/s^2
T	Kinetic energy	J
V	Potential energy	J
W_{nc}	Non-conservative work of external force and moments	J
$\dot{\boldsymbol{\varphi}}_b$	Bit angular velocity	rad/s
V_0	Axial speed of the drill string	m/s
$\dot{\boldsymbol{\varphi}}_{f_t}$	Rotational speed of mud particle	rad/s
T_d	Damping torque of drilling mud	N.m
T_b	Bit rock interaction torque	N.m
$\boldsymbol{\Psi}(x,t)$	Elastic deformation of the drill string	rad
$\boldsymbol{\psi}(x)$	Mode shape function	m
$\boldsymbol{s}(t)$	Corresponding time-dependent	s
$\dot{u}_r$	Axial velocity of moving coordinate system	m/s

1. Introduction

The global demand for energy, coupled with the depletion of accessible shallow reservoirs, has driven drilling operations to greater depths, where the challenges associated with wellbore stability and drill string vibrations have become more pronounced. As drilling depths increase, the severity of vibrations in the drill string—comprising axial, torsional, and lateral motions—becomes a significant concern, as these vibrations can lead to premature equipment failure, increased operational costs, and reduced efficiency. These adverse effects highlight the critical need for effective vibration management to ensure the safety and economic viability of drilling operations [1-5].

A schematic representation of a rotary drilling system, illustrating its key components, including the drill collars, drill pipes, stabilizers, drilling mud, and drill bit, is shown in Figure 1. This system is subjected to complex dynamic interactions, where vibrations in the drill string are influenced by multiple factors, including mechanical properties of the materials, forces from the drilling process, and the interaction between the drill string and the wellbore wall. These vibrations, particularly those involving axial, torsional, and lateral modes, have been extensively studied as they can significantly affect the overall performance and life of the drilling system [6-11]. In particular, failure of the drill string, often resulting from excessive vibration, can lead to costly and time-consuming interventions such as fishing operations, making the analysis and mitigation of these vibrations a key concern in modern drilling operations[1, 6].

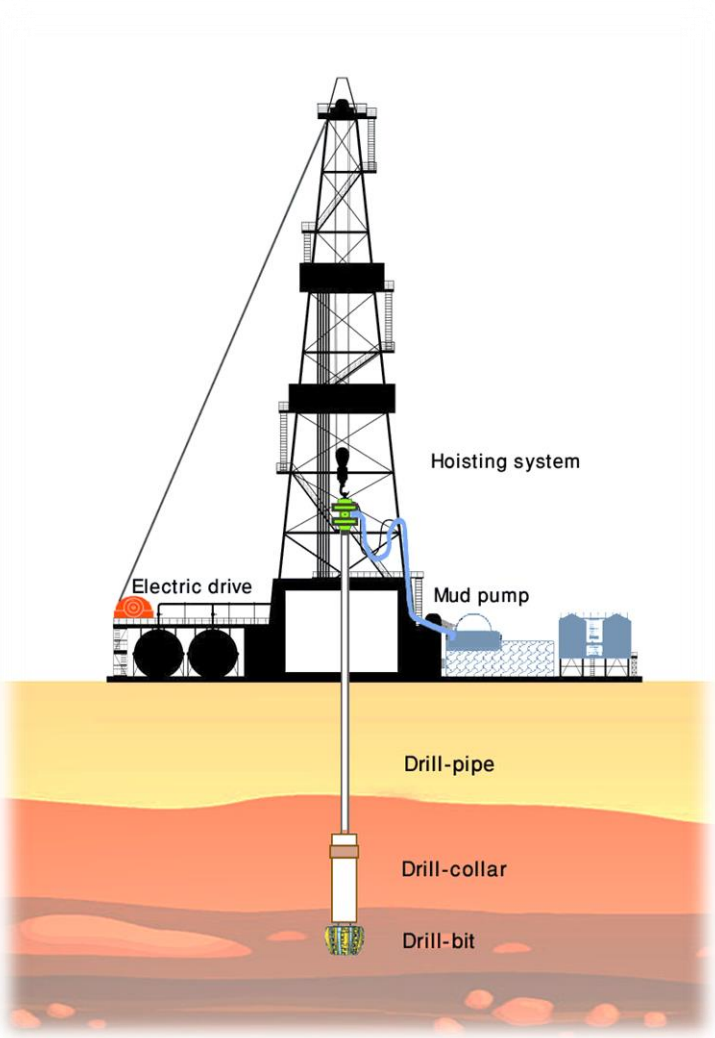

Figure 1. schematic process of rotary drilling

The phenomenon of drill string vibrations, including bit bouncing, stick-slip, and whirling, is inherently tied to complex interactions between various components of the drilling system. Stick-slip and bit-rock interactions, for example, are significant contributors to torsional vibrations, while lateral vibrations are commonly induced by unbalanced forces or the interaction between the drill string and wellbore[7, 9]. These vibrations not only decrease the rate of penetration but also increase the risk of catastrophic failures, which can extend drilling times and increase costs. The research has thus focused on improving the accuracy of dynamic models that can simulate these vibrational phenomena under a wide range of operational conditions[8, 9, 11-13].

Drilling mud plays a pivotal role in the operation of the drilling system by providing cooling for the drill bit, enhancing the rate of penetration, and removing cuttings from the wellbore. However, the rheological properties of the drilling mud—especially its non-Newtonian behavior—can significantly influence the dynamic response of the drill string and its vibration modes. Recent studies have considered the role of mud's viscosity, inertia, and other properties in the context of

drill string dynamics, revealing that mud affects both axial and torsional vibrations in nonlinear ways [14-17]. The complex interaction between mud and drill string vibrations must therefore be taken into account when modeling drilling systems, especially in deep wells where the mud properties can have a pronounced impact on the system's performance.

Advancements in drill string modeling have emphasized the importance of considering coupled vibration modes in more complex, nonlinear models. Early models often treated axial and torsional motions separately, but more recent studies have highlighted the necessity of integrating these modes to capture the full range of dynamic behaviors that occur during drilling operations[13, 18-23]. The incorporation of state-dependent delay equations to represent bit-rock interactions has been particularly valuable in improving the accuracy of these models, as this approach better reflects the complex and time-varying nature of the drilling process[7]. Additionally, considering the effects of non-Newtonian drilling mud behavior, particularly using the Herschel-Bulkley model, allows for a more realistic representation of the rheological forces acting on the drill string during operation. Recently, Bakhtiari-Nejad et al.[24] Conducted the stability analysis of a drill string whose axial and torsional motions were coupled by the bit-rock interaction. In this dynamic model, the motion of drill string was decomposed into the rigid-body and elastic components. They generated the stability diagram and accordingly studied the effect of rock parameters on the stability of system.

While our current study primarily employs a semi-analytical approach to address the nonlinear dynamics of the drill string system with state-dependent delays, it is important to acknowledge the potential role of the Finite Element Method (FEM) in similar complex systems. Recent advances have demonstrated FEM's effectiveness in addressing vibration, stability, and structural analyses involving nonlinear materials, complex geometries, and variable boundary conditions[25-28]. Studies have successfully applied FEM to functionally graded and porous structures, as well as thermally influenced and geometrically imperfect systems[29-31]. Although our model's use of state-dependent delay differential equations presents challenges for direct FEM implementation due to their infinite-dimensional state space, we acknowledge that FEM could provide complementary spatial resolution and detailed mechanical insight, particularly when extended to coupled physical domains. Future research may explore a hybrid framework that integrates FEM with delay-based analytical techniques to capture both the spatial and temporal complexities of such nonlinear drilling systems.

The novelty of the present study lies in the development of a comprehensive nonlinear model that couples both axial and torsional motions of the drill string. This model incorporates state-dependent delay equations to account for the time-dependent bit-rock interaction, as well as the effects of non-Newtonian drilling mud on the system's vibrations. The study employs a semi-discretization method for stability analysis, offering new insights into the stability boundaries of the drilling system under a range of operational conditions. By considering the interplay between drill string dynamics, bit-rock interaction, and mud rheology, this study aims to identify the optimal operational parameters that minimize the risk of instability and enhance drilling efficiency.

2. Nonlinear Dynamic Modelling

As it is shown in Figure 2, the drill string is divided into two sections, the upper part, indexed by subscript 1, which consists of a set of drilling pipes of length L_1, and the lower part which is corresponding to the equipment inside the wellbore and the drill collar with the length of L_2, which is denoted by subscript 2. In the space between the drill string and the wellbore, the drilling mud exists, and the string moves downward. The sections have different cross-sectional areas, and it is assumed that, at the junction of section, the displacements, forces and torques are equal on both sides, and thus, they remain continuous. Hence, two coordinate frames are used to derive the equations, the *Xyz* coordinate frame, which is fixed to the hoisting system, and the *xyz* coordinate frame which is moving with the drill string.

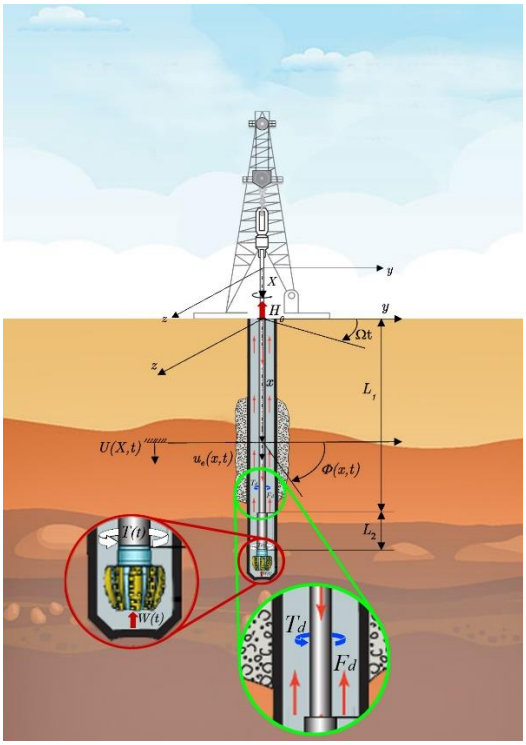

Figure 2. Force and moment applied on a drill string

The axial displacement of an arbitrary point of the drill string with respect to the *Xyz* coordinate system is denoted by $U(X,t)$, which equals

$$\mathrm{U(X,t)} = \mathrm{u_r} + \mathrm{u_e(x,t)} \tag{1}$$

in which, $u_r(t)$ and $u_e(x,t)$ are related to the rigid body motion and the elastic deformation of the drill string along the axial direction, respectively. The axial elastic deformation is considered relative to the moving coordinate system. The equation of motion of the drill string can be derived by resorting to the extended Hamilton's principle, namely,

$$\int_{t1}^{t2} \delta(\mathrm{T} - \mathrm{V} + \mathrm{W_{nc}})\mathrm{dt} = 0 \tag{2}$$

in which, T is the kinetic energy, V is the potential energy and W_{nc} is the non-conservative work of the external forces and moments. The kinetic energy of a drill string can be readily obtained as,

$$T = \frac{1}{2}\int_0^L (\rho A\left(\frac{\partial U}{\partial t}\right)^2 + \rho J\left(\frac{\partial \varphi}{\partial t}\right)^2)dx \quad (3)$$

where ρ is the density of drill string, A is the cross-sectional area, and J is the polar moment of inertia of drill string. Since the coordinate system xyz is moving with the drill string, the time derivatives of $u_e(t)$ and $\varphi(x,t)$ are calculated as follows,

$$\frac{\partial U}{\partial t} = \dot{u}_r + \frac{\partial u_e}{\partial t} + \dot{u}_r \frac{\partial u_e}{\partial x} \quad (4)$$

$$\frac{\partial \varphi}{\partial t} = \frac{\partial \varphi}{\partial t} + \dot{u}_r \frac{\partial \varphi}{\partial x} \quad (5)$$

where $\dot{u}_r$ is the velocity of moving coordinate system in the longitudinal direction. Hence, by substitution of Eqs. (4) and (5) into Eq. (3), the kinetic energy can be obtained as

$$T = \frac{1}{2}\int_0^L (\rho A\left(\dot{u}_r + \frac{\partial u_e}{\partial t} + \dot{u}_r \frac{\partial u_e}{\partial x}\right)^2 + \rho J\left(\frac{\partial \varphi}{\partial t} + \dot{u}_r \frac{\partial \varphi}{\partial x}\right)^2)dx \quad (6)$$

Due to torsional and longitudinal deformations of the drill string, the elastic potential energy can be written as,

$$V = \frac{1}{2}\int_0^L EA\left(\frac{\partial u_e}{\partial x}\right)^2 dx + \frac{1}{2}\int_0^L GJ\left(\frac{\partial \varphi}{\partial x}\right)^2 dx \quad (7)$$

in which E and G are Young's and shear modulus of the drill string material, respectively.

In this study, the viscosity damping effect of drill mud is considered based on the Herschel-Bulkley model[32]. This model explains the non-Newtonian relation between the viscosity and shear rate of material as it follows,

$$\tau = \tau_{Hy} + k_f(\dot{\gamma})^{n_f} \quad (8)$$

in which k_f, n_f and τ_{Hy} are the consistency index, the power-law exponent and the Herschel-Bulkley yield stress, respectively. Consequently, the nonlinear axial damping force of drill mud can be calculated from the following equation [33],

$$F_d = A_d\tau_{Hy} + k_f A_d\left(\frac{V}{\Delta}\right)^{n_f} \quad (9)$$

in which, F_d denotes the shear force, $A_d = 2\pi\frac{d}{2}L$ is the contact surface between mud and drill string and $\Delta = \frac{d_{well}-d}{2}$ is the thickness of the mud layer between the wellbore wall and the drill string. The parameter V is the mud flow rate which is equal to the velocity of drill string component, assuming free slip condition at the contact point of mud and drill. Subsequently, the nonlinear torsional torque due to the rotational damping torque, affected by the rotational speed $\dot{\phi}_{f_t}$, is obtained as,

$$T_d = r_d\left[A_d\tau_{Hy} + k_f A_d\left(\frac{r_d\dot{\phi}_{f_t}}{\Delta}\right)^{n_f}\right] \quad (10)$$

There are also external forces and torques due to the interaction of bit and rock at the tip of the string. In fact, the cutting process consists of two steps, the friction between the bit and rock, and

cutting at the bit and rock face [34]. Therefore, the contact forces and torques are composed of two parts, namely,

$$W_b(t) = W_f + W_c \tag{1}$$

$$T_b(t) = T_f + T_c \tag{2}$$

In which subscripts *f* and *c* denote the components related to the frictional and cutting process, respectively. According to the research of Detournay and Defourny [34], the abovementioned components are obtained as,

$$W_f = \sigma a l H(d) H(\dot{u}) \tag{3}$$

$$W_c = a\epsilon\zeta d(t) H(\dot{\varphi}_b) H(d) \tag{4}$$

$$T_f = \frac{1}{2} a^2 \varepsilon \gamma l \mu(\dot{\varphi}_b) H(d) sgn(\dot{\varphi}_b) H(\dot{u}) \tag{5}$$

$$T_c = \frac{1}{2} a^2 \varepsilon\, d(t) H(\dot{\varphi}_b) H(d) \tag{6}$$

where *H* and *sgn* denote the Heaviside and sign functions, respectively, a is the bit radius, σ is the maximum contact stress related to the interaction between the wear flat and rock, ε is the intrinsic specific energy related to the rock strength, ζ is the characterization number related to the cutter face inclination and γ is the bit geometry effect. Also, μ is the friction coefficient related to the friction angle between the wear flat and rock which is a function of angular velocity of the bit [35], namely,

$$\mu(\omega_b) = \frac{2}{\pi} \tan^{-1}(c_1 \omega_b) \frac{f_1 - f_0}{1 + c_2 \omega_b} \tag{7}$$

in which ω_b is the bit angular speed, c_1, c_2, f_1 and f_0 are the friction model adjustment parameters. These bit-rock interaction laws couple two dynamic modes of axial and torsional. As it is apparent from Eqs.(4) and (6), both cutting moment and force depend on the depth of cutting edges (blades). For a drill bit with *n* uniform blades, the depth of cutting is calculated as follows,

$$d(t) = n d_n(t) \tag{8}$$

in which $d_n(t)$ denotes the instantaneous cutting depth for one blade. By supposing the rate of penetration of two consecutive blades, $d_n(t)$ is obtained as,

$$d_n(t) = u_b(t) - u_b(t - \tau) \tag{19}$$

where $u_b(t)$ denotes the drill bit displacement in the axial direction at time *t* which is expressed by the following relation,

$$u_b(t) = u_r(t) + u_e(L, t) \tag{9}$$

In Eq.(19), τ is the time duration which is required to rotate two consecutive blades with the amount of $2\pi/n$ radian, namely,

$$\varphi(L, t) - \varphi(L, t - \tau) = \frac{2\pi}{n} \tag{10}$$

Due to the dependence of the cutting forces to the previous motions of the system, state dependent delay appears in the vibration model, which adds to the complexity of the stability analysis of the drilling system.

Finally, by considering the hook load at the top of the string, H_0, and the distributed force due to the gravitational acceleration, $f(x,t)$, the total virtual work of the external forces and moments can be obtained as below,

$$\begin{aligned}\delta W_{nc_f} = \int_0^L [\, & f(x,t)\delta u_e(x,t) - T(t)\delta\varphi(L,t) - W(t)\delta u_e(L,t) \\ & - H_0\delta u_e(0,t) - F_d(x,t)\delta u_e(x,t) \\ & - T_d(x,t)\delta\varphi(x,t)]dx\end{aligned} \tag{11}$$

By substituting Eqs.(3),(7) and (11) into eq (2), the equations of axial and torsional motions of the drill string, which is subjected to a non-Newtonian Herschel-Bulkley drilling mud model, are obtained, namely,

$$\rho A\left\{\frac{\partial^2 u_e}{\partial t^2} + \dot{u}_r^2\frac{\partial^2 u_e}{\partial x^2} + \ddot{u}_r\left(1+\frac{\partial u_e}{\partial x}\right) + 2\dot{u}_r\frac{\partial^2 u_e}{\partial x\,\partial t}\right\} = f(x,t) + EA\frac{\partial^2 u_e}{\partial x^2} - F_d(x,t) \tag{12}$$

$$\rho J\left\{\frac{\partial^2\varphi}{\partial t^2} + \ddot{u}_r\frac{\partial\varphi}{\partial x} + 2\dot{u}_r\frac{\partial^2\varphi}{\partial x\,\partial t} + \dot{u}_r^2\frac{\partial^2\varphi}{\partial x^2}\right\} = GJ\,\frac{\partial^2\varphi}{\partial x^2} - T_d(x,t) \tag{13}$$

The corresponding boundary conditions are also expressed as following,

$$\begin{aligned} EA_1\frac{\partial u_e(0,t)}{\partial x} &= H_0 \quad , \quad EA_2\frac{\partial u_e(L,t)}{\partial x} = -W(t) \\ \dot{\varphi}(0,t) &= \Omega \quad , \quad GJ_2\frac{\partial\varphi(L,t)}{\partial x} = -T(t)\end{aligned} \tag{14}$$

where Ω is the nominal rotary speed of the drill string, L is the total length of the drill pipe and the drill collar sections.

3. Solution Methodology

In order to solve the obtained equations of motion, first, the boundary conditions should be transformed into homogeneous forms. This calls for the following variable transformations,

$$u_e(x,t) = U_s(x) + u(x,t) \tag{15}$$

$$\varphi(x,t) = \Omega t + \varphi_s(x) + \Psi(x,t) \tag{27}$$

In the above relations, $U_s(x)$ and $\varphi_s(x)$ represent the steady state drill string axial and torsional elastic displacements, respectively. To obtain the governing equations in terms of these new variables, the time derivatives must be removed from the Eqs.(12) and (13), which leads to the following equations,

$$\rho AV^2\frac{\partial^2 U_s(x)}{\partial x^2} = f(x,t) + EA\frac{\partial^2 U_s(x)}{\partial x^2} - A_d\tau_{Hy} - A_d k_f\left(\frac{V}{\Delta}\right)^{n_f} \tag{28}$$

$$\rho JV^2\frac{\partial^2\varphi_s(x)}{\partial x^2} = GJ\frac{\partial^2\varphi_s(x)}{\partial x^2} - r_d A_d\tau_{HY} - r_d A_d k_f\left(\frac{r_d\Omega}{\Delta}\right)^{n_f} \tag{29}$$

By substitution of the defined variables into Eq.(14), the boundary conditions are reformatted as,

$$EA_1\frac{\partial U_s(0)}{\partial X}=H_0 \quad , \quad EA_2\frac{\partial U_s(L)}{\partial X}=-W_0$$
$$\varphi_s(0)=0 \quad , \quad GJ_2\frac{\partial \varphi_s(L)}{\partial x}=-T_0 \tag{30}$$

in which

$$T_0=\frac{1}{2}a^2\varepsilon\, d_0+\frac{1}{2}a^2\varepsilon\gamma l\,\mu(\Omega) \tag{16}$$

$$W_0=\sigma a l+a\epsilon\zeta d_0 \tag{17}$$

where T_0 and W_0 are the steady state torque and WOB. From Eq.(17), it results that

$$d_0=\frac{W_0-\sigma a l}{a\epsilon\zeta} \tag{18}$$

The parameter d_0 represents the steady state cutting depth, and W_0 can be obtained from the Newton's second law of motion in the axial direction and in the steady-state condition, namely,

$$W_0=Mg-H_0 \tag{19}$$

By substituting Eqs (15) and (27) into Eqs (12) and (13), and by resorting to Eqs. (28) and (29), the following differential equations can be obtained,

$$\rho A\left[\frac{\partial^2 u}{\partial t^2}+2\dot{u}_r\frac{\partial^2 u}{\partial x\,\partial t}+\ddot{u}_r\left(1+\frac{\partial u}{\partial x}\right)+\dot{u}_r^2\frac{\partial^2 u}{\partial x^2}\right]=\rho A(V^2-\dot{u}_r^2)\frac{\partial^2 U_s}{\partial x^2}+EA\frac{\partial^2 u}{\partial X^2}-\rho A\ddot{u}_r\frac{\partial U_s}{\partial x}+A_d k_f\left[\left(\frac{V}{\Delta}\right)^{n_f}-\left(\frac{\dot{u}_r+\dot{u}(x,t)}{\Delta}\right)^{n_f}\right] \tag{20}$$

$$\rho J\left\{\frac{\partial^2\Psi}{\partial x^2}+\dot{u}_r^2\frac{\partial^2\Psi}{\partial x^2}+\ddot{u}_r\frac{\partial\Psi}{\partial x}+2\dot{u}_r\frac{\partial^2\Psi}{\partial x\,\partial t}\right\}=\rho J(V^2-\dot{u}_r^2)\frac{\partial^2\varphi_s}{\partial x^2}+GJ\frac{\partial^2\Psi}{\partial x^2}-\rho J\ddot{u}_r\frac{\partial\varphi_s}{\partial x}+r_d^{n+1}A_d k_f\left[\left(\frac{\Omega}{\Delta}\right)^{n_f}-\left(\frac{\Omega+\Psi(x,t)}{\Delta}\right)^{n_f}\right] \tag{21}$$

Moreover, with the Newton's second law in the axial direction, the rigid body acceleration of the drill string can be obtained as,

$$\ddot{u}_r=g-\frac{H_0}{M}-\frac{W(t)}{M} \tag{37}$$

in which M is the total mass of drill string, g is the gravity acceleration, H_0 is the upward hook load applied on the top of the drill string, and $W(t)$ is the bit-rock interaction force applied on the bit. The rigid body acceleration $\ddot{u}_r$ in Eqs. (20) and (21) can now be replaced with the above relation. In terms of the defined variables u and Ψ, the boundary conditions of Eq. (14) are represented as following,

$$\begin{cases} EA_1 \dfrac{\partial u(0,t)}{\partial x} = 0 \\ \dfrac{\partial \Psi}{\partial t}(0,t) = 0 \\ EA_2 \dfrac{\partial u(L,t)}{\partial x} = -(W(t) - W_0) \\ GJ_2 \dfrac{\partial \Psi}{\partial x}(L,t) = -(T(t) - T_0) \end{cases} \tag{38}$$

In order to solve the obtained equations (Eqs.(20) and (21)) under the foregoing boundary conditions, the Galerkin's method is incorporated. For this purpose, the linear mode shapes of the drill string, which were obtained by Bakhtiari-Nejad and Hosseinzadeh [24], are incorporated.

Modal Analysis of the Linear Model

For obtaining the linear mode shapes of the drill string, the nonlinear terms should be first eliminated from Eqs.(20) and (21), namely,

$$\rho A \frac{\partial^2 u}{\partial t^2} = EA \frac{\partial^2 u}{\partial x^2} \tag{39}$$

$$\frac{\partial^2 \Psi}{\partial t^2} = c_t{}^2 \frac{\partial^2 \Psi}{\partial x^2}, \quad c_t{}^2 = G/\rho \tag{40}$$

Due to the synchronous vibration of drill string, the following solutions can be assumed,

$$u(x,t) = e^{i\omega t}\eta(x) \tag{22}$$

$$\Psi(x,t) = e^{i\omega t}\psi(x) \tag{23}$$

where $\eta(x)$ and $\psi(x)$ are the linear mode shapes of the axial and torsional motions, respectively. By substitution of Eqs.(22) and (23) into Eqs.(39) and (40), and elimination of non-zero exponential time function, two eigenvalue problems are obtained. The eigenfunctions $\eta(x)$ and $\psi(x)$ which satisfy the corresponding eigenvalue problems, considering the boundary conditions at both ends and displacement continuity at the junction, are represented below [24],

$$\begin{aligned} \eta(x) &= \begin{cases} G_1 \cos(p_{ax}x), & x < L_1 \\ F_2 \sin(p_{ax}(x - L_1)) + G_2 \cos(p_{ax}(x - L_1)) & L_1 < x < L \end{cases} \\ G_2 &= G_1 \cos(p_{ax}L_1) \\ F_2 &= -\frac{A_1}{A_2} G_1 \sin(p_{ax}L_1) \end{aligned} \tag{24}$$

$$\begin{aligned} \psi(x) &= \begin{cases} D_1 \sin(p_t x), & x < L_1 \\ D_2 \sin(p_t(x - L_1)) + E_2 \cos(p_t(x - L_1)) & L_1 < x < L \end{cases} \\ E_2 &= D_1 \sin(p_t L_1) \\ D_2 &= \frac{J_1}{J_2} D_1 \cos(p_t L_1) \end{aligned} \tag{25}$$

In which p_{ax} and p_t are the characteristic values of the axial and torsional vibrations. These values are obtained from the characteristic equations of the corresponding eigenvalue problems, namely,

$$-\frac{A_1}{A_{2_1}} \sin(p_{ax}L_1)\cos(p_{ax}L_2) - \cos(p_{ax}L_1)\sin(p_{ax}L_2) = 0 \tag{26}$$

$$\frac{J_1}{J_2}\cos(p_t L_1)\cos(p_t L_2) - \sin(p_t L_1)\sin(p_t L_2) = 0 \tag{27}$$

The linear mode shapes are then utilized to approximate the axial and torsional displacements, namely,

$$\begin{aligned} u(x,t) &= \sum_{j=1}^{M} \eta_j(x) r_j(t) = \boldsymbol{\eta}^T(x)\,\mathbf{r}(t) \\ \psi(x,t) &= \sum_{j=1}^{N} \psi_j(x) s_j(t) = \boldsymbol{\psi}^T(x)\,\mathbf{s}(t)\ , \end{aligned} \tag{47}$$

In which $\eta_j(x)$ and $\psi_j(x)$ denote the j-th mode shape functions of the axial and torsional vibration of the drill string, and $r_j(t)$ and $s_j(t)$ are the j-th corresponding time-dependent generalized coordinates. After substitution of Eq.(47) into Eqs. (20) and (21), and using the Galerkin method [24], the discretized equations of motion of the drill string are obtained as following,

$$M\ddot{u}_r = Mg - H_0 - W_b(t) \tag{48}$$

$$\begin{aligned} &\mathbf{M}_1\ddot{\mathbf{r}}(t) + (\mathbf{C}_1 + 2\mathbf{C}_2\dot{u}_r)\dot{\mathbf{r}}(t) \\ &\qquad + [\mathbf{K}_1 + \dot{u}_r^2\mathbf{K}_2 + \ddot{u}_r\mathbf{K}_3]\mathbf{r}(t) = \mathbf{Q}_{x_f} \end{aligned} \tag{49}$$

$$\begin{aligned} &\mathbf{M}_2\ddot{\mathbf{s}}(t) + (\mathbf{C}_3 + 2\dot{u}_r\mathbf{C}_4)\dot{\mathbf{s}}(t) \\ &\qquad + [\mathbf{K}_4 + \dot{u}_r^2\mathbf{K}_5 + \ddot{u}_r\mathbf{K}_6]\mathbf{s}(t) = \mathbf{Q}_{t_f} \end{aligned} \tag{50}$$

in which the generalized forces are

$$\begin{aligned} Q_{x_f} = {} & -\boldsymbol{\eta}(L)(W(t) - W_0) + \rho(V^2 - \dot{u}_r^2)\int_0^L A\boldsymbol{\eta}(\xi)U_s''(\xi)d\xi \\ & - \rho\ddot{u}_r\int_0^L A\boldsymbol{\eta}(\xi)\big(1 + U_s'(\xi)\big)\,d\xi \\ & + k_f\int_0^L \frac{A_d}{\Delta^{n_f}}\boldsymbol{\eta}(\xi)\left[V^{n_f} - \left(\dot{u}_r + \boldsymbol{\eta}^T(\xi)\dot{r}(t)\right)^{n_f}\right]d\xi \end{aligned} \tag{28}$$

$$\begin{aligned} Q_{t_f} = {} & -\boldsymbol{\psi}(L)(T(t) - T_0) + \rho(V^2 - \dot{u}_r^2)\int_0^L J\boldsymbol{\psi}(\xi)\varphi_S''(\xi)d\xi \\ & - \rho\ddot{u}_r\int_0^L J\boldsymbol{\psi}(\xi)\varphi_S'(\xi)d\xi \\ & + k_f\int_0^L \frac{r_d^{n_f+1}A_d}{\Delta^{n_f}}\boldsymbol{\psi}(\xi)\left[\Omega^{n_f} - \left(\Omega + \boldsymbol{\psi}^T(\xi)\dot{s}(t)\right)^{n_f}\right]d\xi \end{aligned} \tag{29}$$

and the mass, damping and stiffness matrices are defined below,

$$\int_0^L \qquad\qquad \int_0^L \tag{30}$$

$$\mathbf{K_2} = \rho \int_0^L A\boldsymbol{\eta}\,\boldsymbol{\eta}''^T dx \qquad \mathbf{K_5} = \rho \int_0^L J\boldsymbol{\psi}\boldsymbol{\psi}''^T dx$$

$$\mathbf{K_3} = \rho \int_0^L A\boldsymbol{\eta}\,\boldsymbol{\eta}'^T dx \qquad \mathbf{K_6} = \rho \int_0^L J\boldsymbol{\psi}\boldsymbol{\psi}'^T dx$$

$$\mathbf{C_2} = \rho \int_0^L A\boldsymbol{\eta}\,\boldsymbol{\eta}'^T dx \qquad \mathbf{C_4} = \rho \int_0^L \mathbf{J}\psi\boldsymbol{\psi}'^T dx$$

It is noteworthy to mention that $\boldsymbol{C_1}$ and $\boldsymbol{C_3}$ are the Rayleigh damping matrices which are theoretically considered to take into account the viscous damping effects in the model,

$$\begin{aligned} \mathbf{C}_1 &= \alpha_a \mathbf{M}_1 + \beta_a \mathbf{K}_1 \\ \mathbf{C}_3 &= \alpha_t \mathbf{M}_2 + \beta_t \mathbf{K}_4 \end{aligned} \tag{31}$$

whereα_t, β_t,$\alpha_a$andβ_a are the torsional and axial damping ratio tuning coefficients. Hence, by using Eqs. (1) and (17), the excitation terms of Eqs.(28) and (29) can be rewritten in terms of kinematic variables, namely,

$$W(t) - W_0 = a\epsilon\xi(d(t) - d_0) \tag{32}$$

$$T(t) - T_0 = \frac{1}{2}a^2\varepsilon(d(t) - d_0) + \frac{1}{2}a^2\sigma\gamma l[\mu(\Omega + \dot{\Psi}(L,t)) - \mu(\Omega)] \tag{33}$$

Hence, *x(t)* is defined as,

$$x(t) = u_r(t) - V_0 t \tag{57}$$

in which V_0 is the axial steady-state speed which is obtained as,

$$V_0 = \frac{\Omega}{2\pi}\,\frac{W_0 - \sigma a l}{a\epsilon\zeta} \tag{58}$$

By substituting Eq.(57) into Eq.(9) and using new variables of Eq.(15) and Eq. (27), the following relations hold,

$$d_n = x(t) - x(t-\tau) + V_0\tau + u(L,t) - u(L,t-\tau) \tag{59}$$

$$\tau - \tau_0 = -\frac{1}{\Omega}\big(\Psi(L,t) - \Psi(L,t-\tau)\big) \tag{34}$$

Thus, the excitation terms are obtained as,

$$W(t) - W_0 = na\epsilon\zeta\big(u(L,t) - u(L,t-\tau) + V_0(\tau - \tau_0) + x(t) - x(t-\tau)\big) \tag{35}$$

$$T(t) - T_0 = \frac{n}{2}a^2\varepsilon[u(L,t) - u(L,t-\tau) + V_0(\tau - \tau_0) + x(t) - x(t-\tau)] + \frac{1}{2}a^2\sigma\gamma l\left[\mu\left(\Omega + \dot{\Psi}(L,t)\right) - \mu(\Omega)\right] \tag{36}$$

Finally, after Eq.(34) is substituted into Eqs.(35) and (36), and using $x(t)$ instead of $u_r(t)$, the discretized equations of motion of the drill string (Eq. (48)-(50)) can be rewritten in the following forms,

$$M\ddot{x} = -na\epsilon\zeta[u(L,t) - u(L,t-\tau) - \frac{V_0}{\Omega}(\Psi(L,t) - \Psi(L,t-\tau) + x(t) - x(t - \tau)] \tag{37}$$

$$\begin{aligned}&\mathbf{M}_1\ddot{\mathbf{r}}(t) + [\mathbf{C}_1 + 2\mathbf{C}_2(\dot{x} + V_0)]\dot{\mathbf{r}}(t) + [\mathbf{K}_1 + (\dot{x} + V_0)^2\mathbf{K}_2 + \ddot{x}K_3]\mathbf{r}(t) = \\ &-na\epsilon\zeta\boldsymbol{\eta}(L)\left[u(L,t) - u(L,t-\tau) - \frac{V_0}{\Omega}\big(\Psi(L,t) - \Psi(L,t-\tau)\big) + x(t) - x(t - \tau)\right] + \rho(V_0^2 - (\dot{x} + V_0)^2)\int_0^L A\boldsymbol{\eta}(\xi)U_s''(\xi)d\xi - \rho\ddot{x}\int_0^L A\boldsymbol{\eta}(\xi)\big(1 + U_s'(\xi)\big)\,d\xi + \\ &k_f\int_0^L \frac{A_d}{\Delta^{n_f}}\boldsymbol{\eta}(\xi)\left[V_0^{n_f} - \left(\dot{x} + V_0 + \boldsymbol{\eta}^T(\xi)\dot{\mathbf{r}}(t)\right)^{n_f}\right]d\xi\end{aligned} \tag{38}$$

$$\begin{aligned}&\mathbf{M}_2\ddot{\mathbf{s}}(t) + [\mathbf{C}_3 + 2\mathbf{C}_4(\dot{x} + V_0)]\dot{\mathbf{s}}(t) + [\mathbf{K}_4 + (\dot{x} + V_0)^2\mathbf{K}_5 + \ddot{x}\mathbf{K}_6]\mathbf{s}(t) = \\ &-\frac{n}{2}a^2\epsilon\boldsymbol{\psi}(L)\left[u(L,t) - u(L,t-\tau) - \frac{V_0}{\Omega}\big(\Psi(L,t) - \Psi(L,t-\tau)\big) + x(t) - x(t-\tau)\right] - \frac{1}{2}a^2\sigma\gamma l\boldsymbol{\psi}(L)\left[\mu\left(\Omega + \dot{\Psi}(L,t)\right) - \mu(\Omega)\right] + \rho(V_0^2 - (\dot{x} + \\ &V_0)^2)\int_0^L J\boldsymbol{\psi}(\xi)\varphi_S''(\xi)d\xi - \rho\ddot{x}\int_0^L J\boldsymbol{\psi}(\xi)\varphi_S'(\xi)d\xi + k_f\int_0^L \frac{r_d^{n_f+1}A_d}{\Delta^{n_f}}\boldsymbol{\psi}(\xi)\left[\Omega^{n_f} - \left(\Omega + \boldsymbol{\psi}^T(\xi)\dot{S}(t)\right)^{n_f}\right]d\xi\end{aligned} \tag{39}$$

4. Linearization of the Equations of Motion

To represent the equations of motion in terms of only first-order derivatives, $\boldsymbol{z}$, a six-dimensional state vector is defined as,

$$\mathbf{z} = [x\ \mathbf{r}^T\ \mathbf{s}^T\ \dot{x}\ \dot{\mathbf{r}}^T\ \dot{\mathbf{s}}^T]^T \tag{40}$$

Consequently, its derivative is obtained as,

$$\frac{d\mathbf{z}}{dt} = [\dot{x}, \dot{\mathbf{r}}\ \ \dot{\mathbf{s}}, \quad f_1\big(\mathbf{z}, \mathbf{z}(t-\tau)\big), \quad f_2\big(\mathbf{z}, \mathbf{z}(t-\tau)\big), \quad f_3\big(\mathbf{z}, \mathbf{z}(t-\tau)\big)]^T \tag{67}$$

In which f_1 , f_2 and f_3 are obtained from Eqs.(37),(38) and (39) as follows,

$$f_1 = \frac{-na\epsilon\zeta}{M}\left[\boldsymbol{\eta}^T(L)(\mathbf{r}(t) - \mathbf{r}(t-\tau)) - \frac{V_0}{\Omega}\boldsymbol{\psi}^T(L)(\mathbf{s}(t) - \mathbf{s}(t-\tau)) + x(t) - x(t-\tau)\right] \tag{68}$$

$$
\begin{aligned}
f_2 = &-\mathbf{M}_1^{-1}[\mathbf{C}_1 + 2\mathbf{C}_2(\dot{x} + V_0)]\dot{\mathbf{r}}(t) - \mathbf{M}_1^{-1}[\mathbf{K}_1 + (\dot{x} + V_0)^2\mathbf{K}_2 + \ddot{x}\mathbf{K}_3]\mathbf{r}(t) \\
&- na\epsilon\zeta\mathbf{M}_1^{-1}\boldsymbol{\eta}(L)\left[\boldsymbol{\eta}^T(L)(\mathbf{r}(t) - \mathbf{r}(t-\tau)) - \frac{V_0}{\Omega}\boldsymbol{\psi}^T(L)(\mathbf{s}(t)\right. \\
&\left. - \mathbf{s}(t-\tau)) + x(t) - x(t-\tau)\right] \\
&+ \mathbf{M}_1^{-1}\rho(-\dot{x}^2 - 2\dot{x}V_0)\int_0^L A\boldsymbol{\eta}(\xi)U_s''(\xi)d\xi \\
&+ \frac{\rho na\epsilon\zeta}{M}\mathbf{M}_1^{-1}\left[\boldsymbol{\eta}^T(L)(\mathbf{r}(t) - \mathbf{r}(t-\tau)) - \frac{V_0}{\Omega}\boldsymbol{\psi}^T(L)(\mathbf{s}(t) - \mathbf{s}(t\right. \\
&\left. - \tau)) + x(t) - x(t-\tau)\right]\int_0^L A\boldsymbol{\eta}(\xi)\left(1 + U_s'(\xi)\right)d\xi \\
&+ k_f\mathbf{M}_1^{-1}\int_0^L \frac{A_d}{\Delta^{n_f}}\boldsymbol{\eta}(\xi)\left[V_0^{n_f} - \left(\dot{x} + V_0 + \boldsymbol{\eta}^T(\xi)\dot{\mathbf{r}}(t)\right)^{n_f}\right]d\xi
\end{aligned}
\tag{69}
$$

$$
\begin{aligned}
f_3 = &-\mathbf{M}_2^{-1}[\mathbf{C}_3 + 2\mathbf{C}_4(\dot{x} + V_0)]\dot{\mathbf{s}}(t) - \mathbf{M}_2^{-1}[\mathbf{K}_4 + (\dot{x} + V_0)^2\mathbf{K}_5 + \ddot{x}\mathbf{K}_6]\mathbf{s}(t) \\
&- \frac{n}{2}a^2\epsilon\mathbf{M}_2^{-1}\boldsymbol{\psi}(L)\left[\boldsymbol{\eta}^T(L)(\mathbf{r}(t) - \mathbf{r}(t-\tau)) - \frac{V_0}{\Omega}\boldsymbol{\psi}^T(L)(\mathbf{s}(t)\right. \\
&\left. - \mathbf{s}(t-\tau)) + x(t) - x(t-\tau)\right] \\
&- \frac{1}{2}a^2\sigma\gamma l\mathbf{M}_2^{-1}\boldsymbol{\psi}(L)\left[\mu\left(\Omega + \dot{\Psi}(L,t)\right) - \mu(\Omega)\right] \\
&+ \rho\mathbf{M}_2^{-1}(-\dot{x}^2 - 2\dot{x}V_0)\int_0^L J\boldsymbol{\psi}(\xi)\varphi_s''(\xi)d\xi \\
&+ \frac{\rho na\epsilon\zeta}{M}\mathbf{M}_2^{-1}\left[\boldsymbol{\eta}^T(L)(\mathbf{r}(t) - \mathbf{r}(t-\tau)) - \frac{V_0}{\Omega}\boldsymbol{\psi}^T(L)(\mathbf{s}(t) - \mathbf{s}(t\right. \\
&\left. - \tau)) + x(t) - x(t-\tau)\right]\int_0^L J\boldsymbol{\psi}(\xi)\varphi_s'(\xi)d\xi \\
&+ k_f\mathbf{M}_2^{-1}\int_0^L \frac{r_d^{n_f+1}A_d}{\Delta^{n_f}}\boldsymbol{\psi}(\xi)\left[\Omega^{n_f} - \left(\Omega + \boldsymbol{\psi}^T(\xi)\dot{S}(t)\right)^{n_f}\right]d\xi
\end{aligned}
\tag{41}
$$

Equation (67) is nonlinear due to the presence of nonlinear functions f_1 , f_2 and f_3. It was proved in [36, 37] that a nonlinear system is asymptotically stable if a linear stability analysis of the steady-state solution of the original system guarantees the asymptotic stability. The steady-state solution of Eq.(67) can be considered as,

$$
\mathbf{Z}_{ss} = \mathbf{O}_{2N\times 2N} \tag{42}
$$

where $\boldsymbol{O}$ is a $2N \times 2N$ zero matrix in which N is obtained as,

$$
N = N_t + N_x + 1 \tag{43}
$$

in which N_t and N_x are the number of employed mode shapes of torsional and axial motion of drill string, respectively. It should be noted that the state-dependent delay linearization, which appeared in Eqs. (37) to (39), was carried out by neglecting its perturbations around the steady state value

[36-38]. The time delay between two consecutive blades, in the steady state condition, is calculated from the following relation,

$$\tau_0 = \frac{2\pi}{n\Omega} \tag{44}$$

Hence, the linear form of Eqs. (48)-(50) is obtained as,

$$\dot{\mathbf{z}}(t) = \mathbf{A}\mathbf{z}(t) + \mathbf{B}\mathbf{y}(\tau - t) \tag{45}$$

where $\boldsymbol{A}$ and $\boldsymbol{B}$ are presented in the Appendix, and $\boldsymbol{y}$ is the state variable vector, namely,

$$\mathbf{z} = [\mathbf{y} \quad \dot{\mathbf{y}}]^T \tag{46}$$

5. Stability Analysis

Dependence of the present and past states of the system on the cutting depth results in a state-dependent delay equation. As a numerical method, a semi-discretization method can be employed to study the stability of delay differential equations (DDE) like Eq. (45). This method is based on the time intervals $[t_i\,, t_{i+1})$ of length discretization step h which is related to the time delay as it follows,

$$h(p + \frac{1}{2}) = \tau_0 \tag{47}$$

where $p \in \mathbb{N}$. Thus, Eq. (45) can be reformatted in terms of time scale $t_i = ih$, $i \in \mathbb{Z}$, namely,

$$\dot{\mathbf{z}} = \mathbf{A}\mathbf{z}(t) + \mathbf{B}\mathbf{y}(t_{i-p})\,, \qquad t \in [t_i\,, t_{i+1}). \tag{77}$$

If the initial conditions $\boldsymbol{z}_i = \boldsymbol{z}(t_i)$ and the delayed state variable $\boldsymbol{y}_{i-p} = \boldsymbol{y}(t_{i-p})$ are given, then the solution of Eq.(77) over one interval $[t_i\,, t_{i+1})$ can be expressed as,

$$\mathbf{z}_{i+1} = \underbrace{e^{\mathbf{A}h}}_{:=\mathbf{P}}\mathbf{z}_i + \underbrace{\int_0^h e^{\mathbf{A}(h-s)}ds\,\mathbf{B}}_{:=\mathbf{R}}\mathbf{y}_{i-p} \tag{78}$$

If $\boldsymbol{A}^{-1}$ exists, then the integration in the right side of the above equation gives,

$$\mathbf{P} = e^{\mathbf{A}h}\,, \mathbf{R} = \left(e^{\mathbf{A}h} - \mathbf{I}\right)\mathbf{A}^{-1}\mathbf{B} \tag{79}$$

in which $\boldsymbol{I}$ is the $n \times n$ identity matrix. Equation (77) implies the following discrete map,

$$\mathbf{z}_{i+1} = \mathbf{G}_i\mathbf{z}_i\,, \mathbf{z}_i = \left(\mathbf{y}_i\ \dot{\mathbf{y}}_i\ \mathbf{y}_{i-1} \dots \dots\ \mathbf{y}_{i-p}\right)^T$$

$$\begin{pmatrix} \mathbf{y_{i+1}} \\ \dot{\mathbf{y}}_{\mathbf{i+1}} \\ \mathbf{y_i} \\ \mathbf{y_{i-1}} \\ . \\ . \\ . \\ \mathbf{y_{i-p+1}} \end{pmatrix} = \underbrace{\begin{pmatrix} \mathbf{P_{11}} & \mathbf{P_{12}} & \mathbf{0} & \mathbf{0} & \dots & \mathbf{0} & \mathbf{R_1} \\ \mathbf{P_{21}} & \mathbf{P_{22}} & \mathbf{0} & \mathbf{0} & \dots & \mathbf{0} & \mathbf{R_2} \\ \mathbf{I} & \mathbf{0} & \mathbf{0} & \mathbf{0} & \dots & \mathbf{0} & \mathbf{0} \\ \mathbf{0} & \mathbf{0} & \mathbf{I} & \mathbf{0} & \dots & \mathbf{0} & \mathbf{0} \\ . & . & . & . & . & . & . \\ . & . & . & . & . & . & . \\ . & . & . & . & . & . & . \\ \mathbf{0} & \mathbf{0} & \mathbf{0} & \mathbf{0} & \dots & \mathbf{I} & \mathbf{0} \end{pmatrix}}_{\mathbf{G}} \begin{pmatrix} \mathbf{y_i} \\ \dot{\mathbf{y}}_{\mathbf{i}} \\ \mathbf{y_{i-1}} \\ \mathbf{y_{i-2}} \\ . \\ . \\ . \\ \mathbf{y_{i-p}} \end{pmatrix} \tag{48}$$

where $\boldsymbol{G}$ is an $(n + pm) \times (n + pm)$ matrix. The stability of the system with Eqs. (48) - (50) can be evaluated by resorting to the eigenvalue analysis of matrix $\boldsymbol{G}$. If the magnitude of all eigenvalues are less than one, then it concludes that the system attains asymptotic stability.

6. Results

The physical characteristics of the under-study drill string are presented in Table 1.

Table 1. Parameter values of drill string used for stability analysis[24]

Parameter	Definition	Value	Unit	Parameter	Definition	Value	Unit
D_o^p	Drill pipe outer Diam.	0.127	m	D_i^p	Drill pipe inner Diam.	0.108	m
D_o^c	Drill collar outer Diam.	0.1524	m	D_i^c	Drill collar inner Diam.	0.0572	m
E	Young's modulus	200	GPa	G	Shear modulus	77	GPa
L_1	Upper part length	1200	m	L_2	BHA length	200	m
ρ	density	8000	kg/m^3	a	Drill bit radius	0.108	m
σ	Max. contact stress	60	MPa	ε	Rock intrinsic specific energy	60	MPa
γ	Drill bit geom. Coef.	1	-	l	Drill bit wear-flat length	1.2	mm
μ_1	Kinetic friction Coef.	1	-	μ_0	Static friction Coef.	1.6	-
ξ_t	Torsional damping ratio	0.0015	-	ζ	Drill bit inclination number	0.6	-

Also, to determine the effect of non-Newtonian mud rheology on the vibration of the drill string, a parametric study, based on the model which was introduced in section 1, will be carried out. In particular, there are researches [39-41] in which the range of mud parameters for Bentonite, Water and Oil-based and Biopolymers muds were presented based on the Herschel-Bulkley non-Newtonian model (Table 2).

Table 2. The ranges of Herschel-Bulkley model parameters[42]

Parameter	Definition	Value range	Unit
n_f	Power-law exponent	0-1	-
k_f	Fluid consistency index	0-5	$Pa\ s^{n_f}$
τ_{Hy}	Herschel-Bulkley yield stress	3-7	Pa

For the aforementioned physical parameters of the drill string and mud, and by resorting to the semi-discretization method, the stable region boundary of drill string is obtained and shown on W_0-Ω plot in Figure 3. In this figure, the area under the curves indicates the stable region. Moreover, the effect of the number of mode shapes on the stability region and the convergence of the stability study is shown. As it is apparent, the first four axial and the first torsional mode shapes are adequate to achieve convergence of the stability areas, as it is shown in the figure. It reveals that the axial mode shapes have a greater influence on the convergence of stability region.
In Figure 3, the vertical line at the value of 15(rad/s) represents the stability limit boundary (threshold) of the drill string rotational velocity, in other words, the system will become unstable if it operates at a lower rate than this value. As it is apparent, the number of mode shapes has no effect on the upper boundary of stable area.

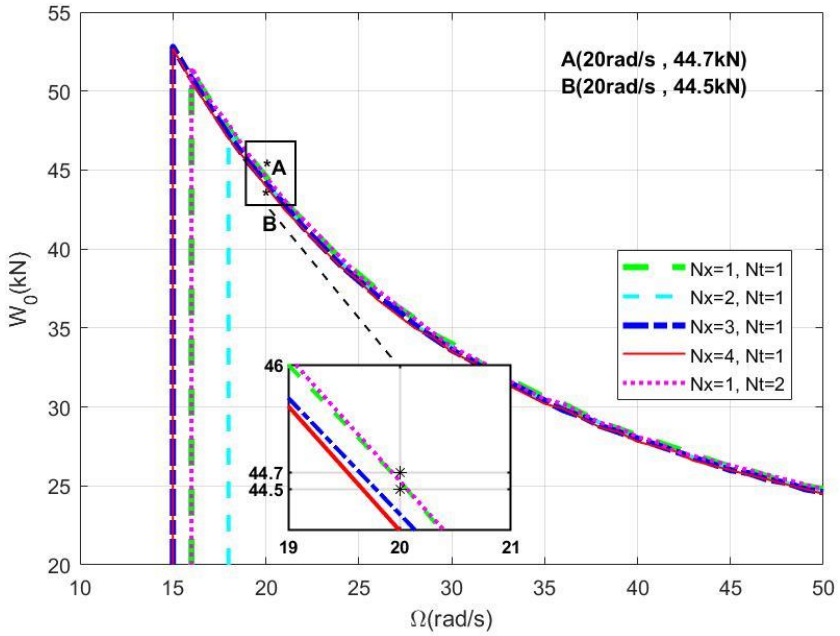

Figure 3.Effect of the number of axial and torsional mode shape on the convergence of the stability boundary

In order to validate the results of the stability analysis and show that a little change in parameters like nominal weight on the bit (W0) leads to system instability, time history of the bit angular velocity is obtained for two different conditions inside and outside the stable region (e.g. points B and A in Figure 3). The evolution of angular bit speed for points B and A are shown in Figure 4

and 5, respectively. Decaying behavior of vibrations in Figure 4(stable drilling) and increasing vibration amplitude in Figure 5(unstable drilling) confirms the result of stability analysis in Figure 3.

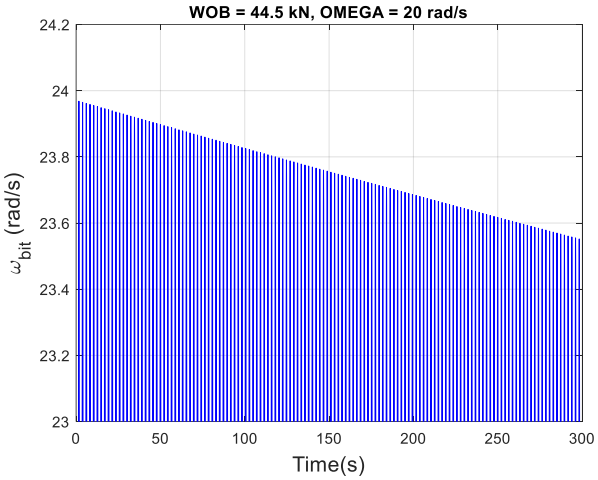

Figure 4. Stable drilling near the boundary of stability (Ω=20 rad/s, W0=44.5 kN).

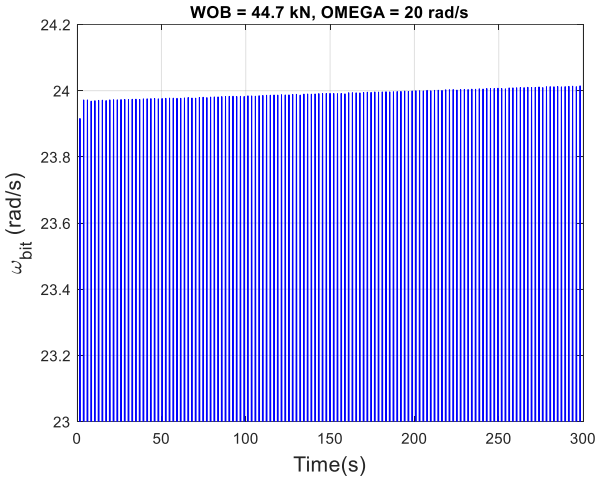

Figure 5.Unstable drilling near the boundary of stability (Ω=20 rad/s, W0=44.7 kN).

6.1 Results Verification

Bakhtiari-Nejad and Hosseinzadeh[24] verified their model, which is here denoted by "ref" model, by comparing the results of a special case (constant axial rigid-body speed) with the ones which were obtained by a model presented by Liu et al.[23]. It was shown that both models produce similar stability boundaries. Therefroe, in order to verify the drilling system model the corresponding solution procedure presented in this study, the results are compared with the ones which were obtained by "ref" model in the absence of mud effect. In this regard, the effect of mud parameters, n_f and k_f, is gradully decreased in the present model, and it is observed that the stability boundaries converge to the ones that was obtained by the ref model, as it is shown in Figure 6. Here, the number of torsional and axial mode shapes is one for this subsection simulation results (N_x=N_t=*1*).

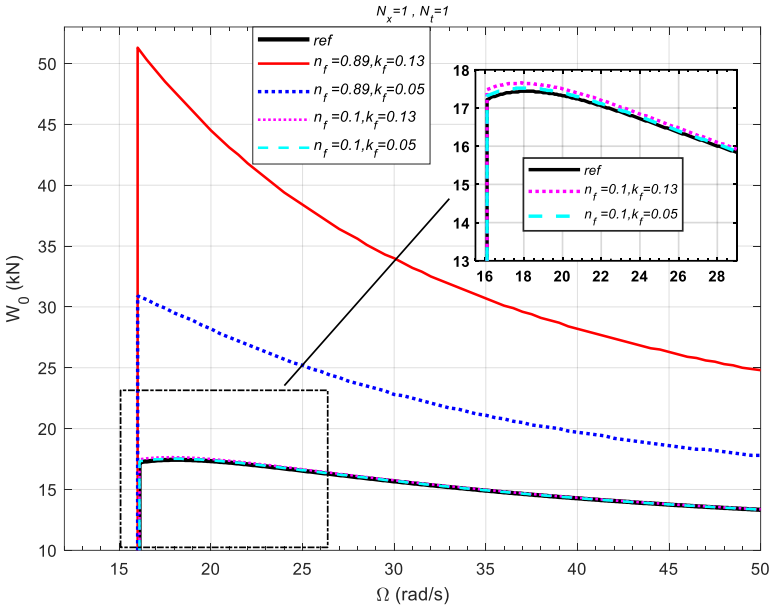

Figure 6. Model verification by comparisons of stability boundaries with the ones which were obtained by the ref[24] model

As it is separately shown in Figure 7, in the case of zero mud parameters, the stability boundaries of both models are completely matched with each other.

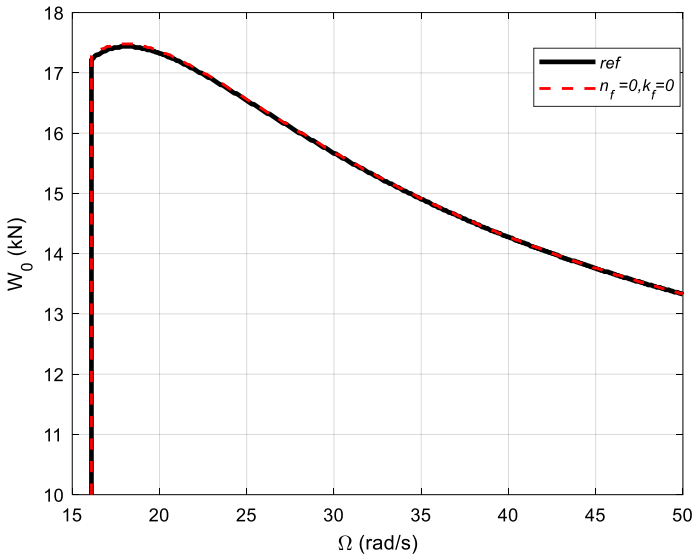

Figure 7. Comparing the obtained stability boundaries of ref model with the ones of model presented in this paper, when n_f and k_f are zero

6.2 Stability Analysis in the Presence of Drill Mud

To provide a more realistic model, this study incorporates the effect of drill mud modeled as a non-Newtonian fluid, extending the earlier work by Bakhtiari-Nejad and Hosseinzadeh [24]. As shown in Figure 8, the presence of mud enlarges the stability region compared to the case without mud. This means that for the same rotational speed, a higher WOB (Weight on Bit) can be tolerated when mud is present, leading to improved drilling performance. The vertical boundary remains

unchanged at 16 rad/s for both cases when using the same mode shapes, indicating the mud's influence primarily affects the upper limit of stability.

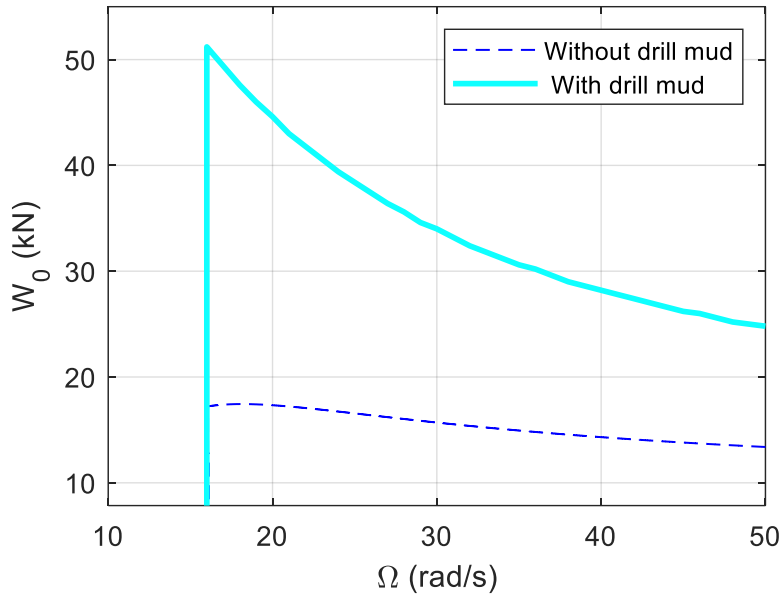

Figure 8.Effec of drill mud damping on stability region

6.3 Parametric Study

The effect of various physical parameters from Table 2 and Table 3 on the stability boundary is evaluated, assuming on torsional and axial mode (N_x=N_t=*1*).

Table 3. Different outer diameters of drill collar and drill pipe

Case number	D_o^c	D_o^p	unit
1	0.1524	0.127	m
2	0.1524	0.147	m
3	0.1724	0.127	m
4	0.1724	0.147	m

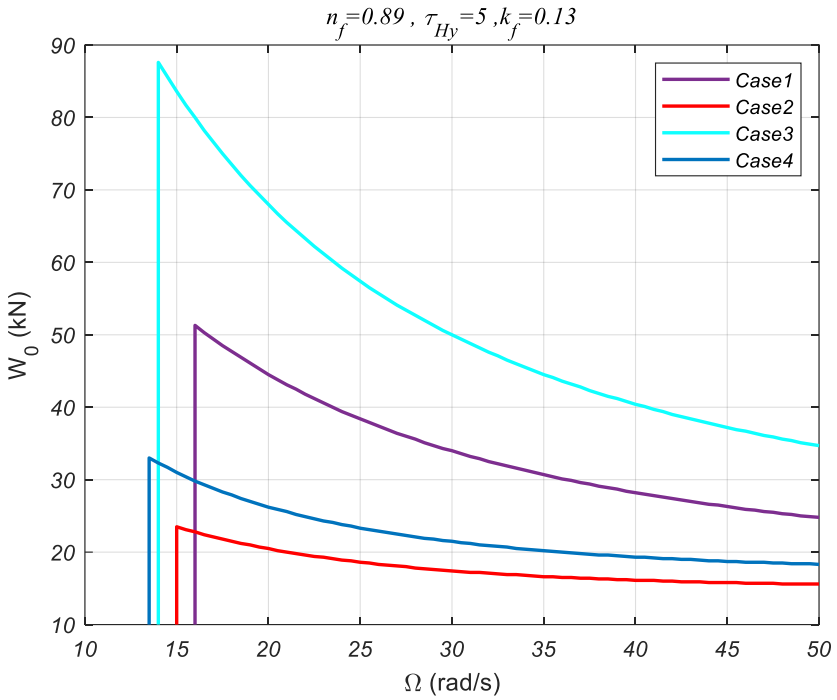

Figure 9.The effect of drill string and drill collar thicknesses on the stability region

- **Pipe and Collar Thickness (Figure 9):**
  Increasing the drill pipe thickness reduces stability at higher WOBs and shifts the onset of instability to lower speeds. In contrast, a thicker drill collar expands the stable region, especially at low speeds, by increasing structural stiffness.
- **Yield Stress (Figure 10):**
  Changing the yield stress of the mud has minimal impact on the stability region. This suggests that the initiation threshold for fluid flow does not significantly alter the dynamic response of the system.

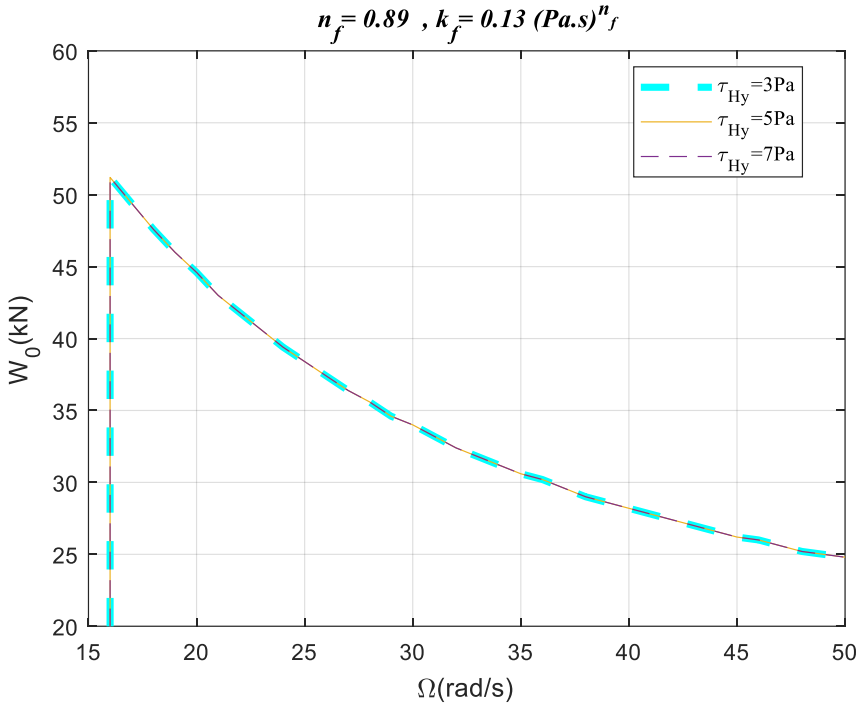

Figure 10.The effect of yield stress (τ_{Hy}) on stability analysis

- **Consistency Index (k_f) – Figure 11:**
  Higher k_f indicates a thicker mud. As k_f increases, both the maximum allowable WOB and the range of stable speeds expand. Physically, the increased damping and resistance provided by more viscous mud suppress vibrations more effectively.

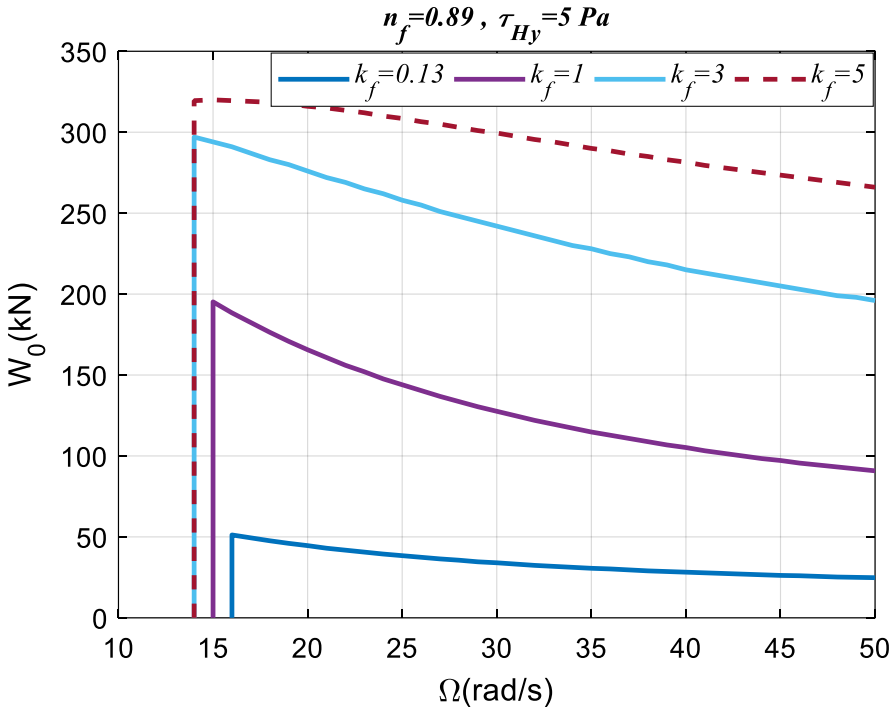

Figure 11.The effect of consistency index on stability analysis

- **Power-Law Index (n_f) – Figure 12:**
  As n_f increases, the mud becomes less shear-thinning. This enhances stability at lower speeds and higher WOBs, shifting both vertical and upper boundaries favorably. However, this effect is more pronounced when nf increases from 0.5 to 1 than in lower ranges.

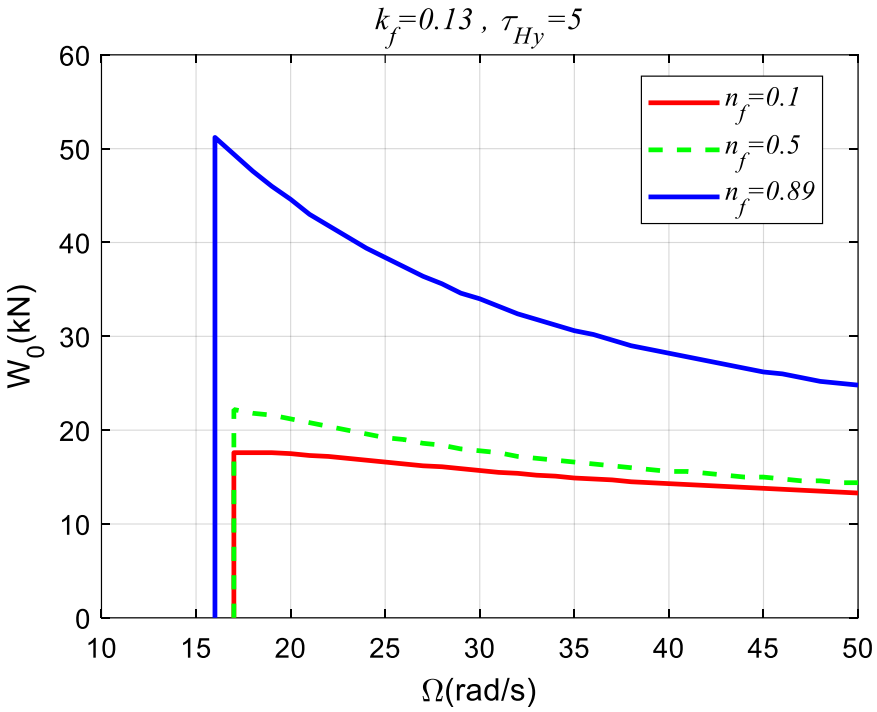

Figure 12.The effect of power-law exponent on stability analysis

- **Damping Effect (Figure 13):**
  Mud damping has a strong stabilizing influence on rotational motion but minimal effect on axial stability. This asymmetry reflects the dominant role of torsional vibrations in drill string instability.

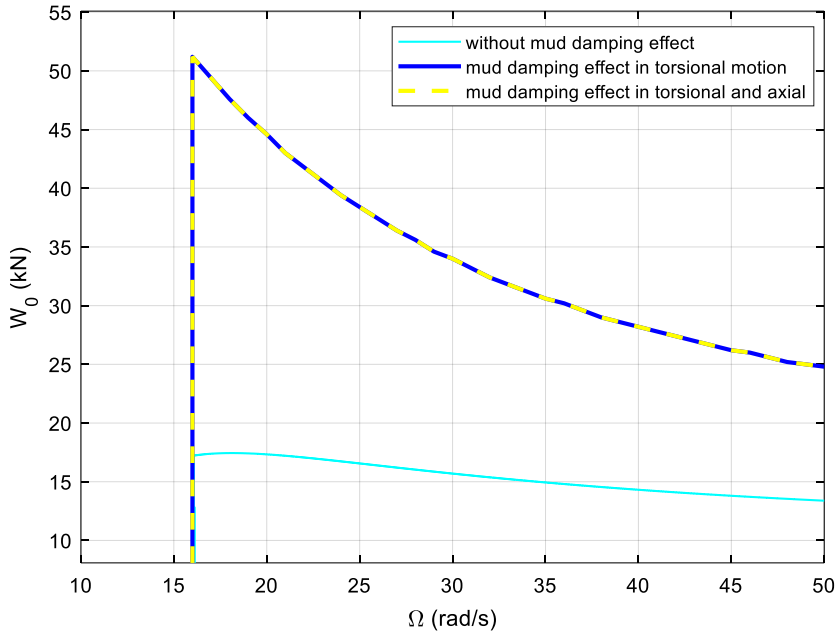

Figure 13.Comparing the effect of mud applied in axial and torsional direction

7. Conclusions

The following conclusions were drawn from the dynamic stability analysis of a drill string interacting with non-Newtonian drilling mud modeled via the Herschel-Bulkley formulation:

- The inclusion of drill mud damping significantly affects the stability boundaries of the drill string system.
- Torsional damping plays a critical role in stability, while axial damping has negligible influence.
- At lower rotational speeds (Ω), the drill string can tolerate higher WOB, enhancing penetration rate.
- The **consistency index (k_f)** and **power-law index (n_f)** significantly expand the stability region:
    - Higher k_f increases both the upper WOB limit and allows for lower operating speeds.
    - Higher n_f also shifts the stability region positively, but its influence is less than k_f.
- The **yield stress** of the mud has no noticeable effect on the system's stability.
- Increasing k_f and n_f shifts the vertical boundary to the left and the upper boundary upward.
- Optimal mud design should aim for high k_f and n_f; however, industrial fluids often require low n_f for appropriate shear-thinning behavior.
- Therefore, in addition to selecting proper mud properties, adaptive control strategies are recommended to maintain drilling stability.

These insights can guide better mud selection and control strategy development for safer and more efficient drilling operations.

Acknowledgments

This study was supported by R&D of Pars Special Economic Energy Zone which is an organization of the National Iranian Oil Company. We would also like to thank the director of R&D of this organization for the valuable technical support on this research work.

Declaration of conflicting interests

The Authors declare that there is no conflict of interest.

ORCID iDs

Kamal Aghadadi https://orcid.org/0000-0002-5951-8264

Uncategorized References

[1] R. Shyu, J. Vandive, J.J.S.D.E. Nicholson, Case studies of the bending vibration and whirling motion of drill collars, SPE(Society of Petroleum Engineers), 5 (1990).

[2] Y. Khulief, F. Al-Sulaiman, S. Bashmal, Vibration analysis of drillstrings with self-excited stick–slip oscillations, Journal of sound and vibration, 299 (2007) 540-558.
[3] T. Richard, C. Germay, E. Detournay, A simplified model to explore the root cause of stick–slip vibrations in drilling systems with drag bits, Journal of sound and vibration, 305 (2007) 432-456.
[4] M. Zamanian, S. Khadem, M. Ghazavi, Stick-slip oscillations of drag bits by considering damping of drilling mud and active damping system, Journal of Petroleum Science and Engineering, 59 (2007) 289-299.
[5] K. Aghadadi, F. Bakhtiari-Nejad, A. Taghvaeipour, A. Hosseinzadeh, Super twisting control of torsional vibration in non-minimum phase nonlinear drill string system, Journal of Vibration and Control, 29 (2023) 4317-4333.
[6] Y. Zhao, A. Noorbakhsh, M. Koopialipoor, A. Azizi, M. Tahir, A new methodology for optimization and prediction of rate of penetration during drilling operations, Engineering with Computers, 36 (2020) 587-595.
[7] T. Richard, C. Germay, E. Detournay, Self-excited stick–slip oscillations of drill bits, Comptes rendus MECANIQUE, 332 (2004) 619-626.
[8] Y. Khulief, F. Al-Sulaiman, S. Bashmal, Vibration analysis of drillstrings with string—borehole interaction, Proceedings of the Institution of Mechanical Engineers, Part C: Journal of Mechanical Engineering Science, 222 (2008) 2099-2110.
[9] N. Mihajlovic, A. Van Veggel, N. Van de Wouw, H. Nijmeijer, Analysis of friction-induced limit cycling in an experimental drill-string system, Journal of Dynamic Systems, Measurement, and Control, 126 (2004) 709-720.
[10] J. Jansen, Non-linear rotor dynamics as applied to oilwell drillstring vibrations, Journal of sound and vibration, 147 (1991) 115-135.
[11] V. Dunayevsky, F. Abbassian, A. Judzis, Dynamic stability of drillstrings under fluctuating weight on bit, SPE drilling completion, 8 (1993) 84-92.
[12] G.H. Van Der Heijden, Bifurcation and chaos in drillstring dynamics, Chaos, Solitons & Fractals, 3 (1993) 219-247.
[13] R. Kazemi, A.A. Jafari, M. Faraji Mahyari, The effect of drilling mud flow on the lateral and axial vibrations of drill string, in: ASME 2010 10th Biennial Conference on Engineering Systems Design and Analysis, American Society of Mechanical Engineers Digital Collection, 2010, pp. 465-473.
[14] C. Germay, N. Van de Wouw, H. Nijmeijer, R. Sepulchre, Nonlinear drillstring dynamics analysis, SIAM Journal on Applied Dynamical Systems, 8 (2009) 527-553.
[15] C. Germay, V. Denoël, E. Detournay, Multiple mode analysis of the self-excited vibrations of rotary drilling systems, Journal of sound and vibration, 325 (2009) 362-381.
[16] V. Gulyayev, O. Borshch, Free vibrations of drill strings in hyper deep vertical bore-wells, Journal of Petroleum Science and Engineering, 78 (2011) 759-764.
[17] T. Ritto, M. Escalante, R. Sampaio, M.B. Rosales, Drill-string horizontal dynamics with uncertainty on the frictional force, Journal of sound and vibration, 332 (2013) 145-153.
[18] A. Christoforou, A. Yigit, Dynamic modelling of rotating drillstrings with borehole interactions, Journal of sound and vibration, 206 (1997) 243-260.
[19] A. Yigit, A. Christoforou, Coupled axial and transverse vibrations of oilwell drillstrings, Journal of sound and vibration 195 (1996) 617-627.
[20] A. Yigit, A. Christoforou, Coupled torsional and bending vibrations of drillstrings subject to impact with friction, Journal of sound and vibration, 215 (1998) 167-181.
[21] A. Ghasemloonia, D.G. Rideout, S.D.J.P.o.t.I.o.M.E. Butt, Part C: Journal of Mechanical Engineering Science, Coupled transverse vibration modeling of drillstrings subjected to torque and spatially varying axial load, 227 (2013) 946-960.

[22] J. Liu, X. Guo, G. Wang, Q. Liu, D. Fang, L. Huang, L. Mao, Bi-nonlinear vibration model of tubing string in oil & gas well and its experimental verification, Applied Mathematical Modelling, 81 (2020) 50-69.
[23] X. Liu, N. Vlajic, X. Long, G. Meng, B. Balachandran, Coupled axial-torsional dynamics in rotary drilling with state-dependent delay: stability and control, Nonlinear Dynamics, 78 (2014) 1891-1906.
[24] F. Bakhtiari-Nejad, A. Hosseinzadeh, Nonlinear dynamic stability analysis of the coupled axial-torsional motion of the rotary drilling considering the effect of axial rigid-body dynamics, International Journal of Non-Linear Mechanics, 88 (2017) 85-96.
[25] Z. Belabed, A. Tounsi, A.A. Bousahla, A. Tounsi, M. Yaylacı, Accurate free and forced vibration behavior prediction of functionally graded sandwich beams with variable cross-section: a finite element assessment, Mechanics Based Design of Structures and Machines, 52 (2024) 9144-9177.
[26] S.A. Meftah, S.M. Aldosari, A. Tounsi, T. Cuong-Le, K.M. Khedher, A.E. Alluqmani, Simplified homogenization technique for nonlinear finite element analysis of in-plane loaded masonry walls, Engineering Structures, 306 (2024) 117822.
[27] A. Tounsi, Z. Belabed, F. Bounouara, M. Balubaid, S. Mahmoud, A.A. Bousahla, A. Tounsi, A finite element approach for forced dynamical responses of porous FG nanocomposite beams resting on viscoelastic foundations, International Journal of Structural Stability and Dynamics, (2024) 2650078.
[28] D.M. Sekban, E.U. Yaylacı, M.E. Özdemir, M. Yaylacı, A. Tounsi, Investigating formability behavior of friction stir-welded high-strength shipbuilding steel using experimental, finite element, and artificial neural network methods, Journal of Materials Engineering and Performance, (2024) 1-9.
[29] Z. Lakhdar, S.M. Chorfi, S.A. Belalia, K.M. Khedher, A.E. Alluqmani, A. Tounsi, M. Yaylacı, Free vibration and bending analysis of porous bi-directional FGM sandwich shell using a TSDT p-version finite element method, Acta Mechanica, 235 (2024) 3657-3686.
[30] B.M. Cuong, A. Tounsi, N.T.H. Van, P. Van Minh, Finite element modelling for the static bending response of rotating FG-GPLRC beams with geometrical imperfections in thermal mediums, Computers and Concrete, 33 (2024) 91-102.
[31] V. Katiyar, A. Gupta, A. Tounsi, Microstructural/geometric imperfection sensitivity on the vibration response of geometrically discontinuous bi-directional functionally graded plates (2D FGPs) with partial supports by using FEM, Steel and Composite Structures, An International Journal, 45 (2022) 621-640.
[32] W.H. Herschel, R. Bulkley, Konsistenzmessungen von gummi-benzollösungen, Kolloid-Zeitschrift, 39 (1926) 291-300.
[33] W.C. Lyons, G.J. Plisga, Standard handbook of petroleum and natural gas engineering, Third Edition ed., Elsevier, 2016.
[34] E. Detournay, P. Defourny, A phenomenological model for the drilling action of drag bits, in: International journal of rock mechanics and mining sciences & geomechanics abstracts, Elsevier, 1992, pp. 13-23.
[35] R. Leine, D. Van Campen, A. De Kraker, L. Van Den Steen, Stick-slip vibrations induced by alternate friction models, Nonlinear dynamics, 16 (1998) 41-54.
[36] F. Hartung, Linearized stability in periodic functional differential equations with state-dependent delays, Journal of Computational and Applied Mathematics, 174 (2005) 201-211.
[37] K. Nandakumar, M. Wiercigroch, Stability analysis of a state dependent delayed, coupled two DOF model of drill-stringvibration, Journal of sound and vibration, 332 (2013) 2575-2592.
[38] T. Insperger, G. Stépán, J. Turi, State-dependent delay in regenerative turning processes, Nonlinear Dynamics, 47 (2007) 275-283.
[39] V. Kelessidis, R. Maglione, C. Tsamantaki, Y. Aspirtakis, Optimal determination of rheological parameters for Herschel–Bulkley drilling fluids and impact on pressure drop, velocity profiles and penetration rates during drilling, Journal of Petroleum Science and Engineering, 53 (2006) 203-224.
[40] J. Davison, S. Clary, A. Saasen, M. Allouche, D. Bodin, V. Nguyen, Rheology of various drilling fluid systems under deepwater drilling conditions and the importance of accurate predictions of downhole

fluid hydraulics, in: SPE Annual Technical Conference and Exhibition, Society of Petroleum Engineers, 1999.
[41] S.B. Hamed, M. Belhadri, Rheological properties of biopolymers drilling fluids, Journal of Petroleum Science and Engineering, 67 (2009) 84-90.
[42] A. Guzek, I. Shufrin, E. Pasternak, A.V. Dyskin, Influence of drilling mud rheology on the reduction of vertical vibrations in deep rotary drilling, Journal of Petroleum Science and Engineering, 135 (2015) 375-383.

Appendix

The matrix $\boldsymbol{A}$ and $\boldsymbol{B}$ in Eq.(45) are presented as follows,

$$\boldsymbol{A}=\begin{bmatrix}A_1\\A_2\\A_3\\A_4\end{bmatrix},\qquad \boldsymbol{B}=\begin{bmatrix}B_1\\B_2\\B_3\\B_4\end{bmatrix}.$$

in which matrix element $\boldsymbol{A}$, $\boldsymbol{B}$ calculated in the following way,

$$A_1=[O_{N\times N}\qquad I_{N\times N}]$$

$$A_2=-\frac{na\epsilon\zeta}{M}\begin{bmatrix}1 & \eta^T(L) & -\frac{V_0}{\Omega}\psi^T(L) & O_{1\times N}\end{bmatrix}$$

$$A_2=-\frac{na\epsilon\zeta}{M}\begin{bmatrix}1 & \eta^T(L) & -\frac{V_0}{\Omega}\psi^T(L) & O_{1\times N}\end{bmatrix}$$

$$A_3=[A_{31}\quad A_{32}\quad A_{33}\quad A_{34}\quad A_{35}\quad A_{36}]$$

$$A_{31}=-na\epsilon\zeta M_1^{-1}\eta(L)+\frac{\rho na\epsilon\zeta}{M}M_1^{-1}\int_0^L A\eta(\xi)\big(1+U_s'(\xi)\big)\,d\xi$$

$$A_{32}=-M_1^{-1}[K_1+V_0^2K_2]-na\epsilon\zeta M_1^{-1}\eta(L)\eta^T(L)+\frac{\rho na\epsilon\zeta}{M}M_1^{-1}\left[\int_0^L A\eta(\xi)\big(1+U_s'(\xi)\big)\,d\xi\right]\eta^T(L)$$

$$A_{33}=\frac{na\epsilon\zeta}{\Omega}V_0M_1^{-1}\eta(L)\psi^T(L)-\frac{\rho na\epsilon\zeta}{M}\frac{V_0}{\Omega}M_1^{-1}\left[\int_0^L A\eta(\xi)\big(1+U_s'(\xi)\big)\,d\xi\right]\psi^T(L)$$

$$A_{34}=-2\rho V_0M_1^{-1}\int_0^L A\eta(\xi)U_s^{"}(\xi)d\xi-n_fk_fV_0^{n_f-1}M_1^{-1}\int_0^L\frac{A_d}{\Delta^{n_f}}\eta(\xi)\,d\xi$$

$$A_{35}=\ -M_1^{-1}[C_1+2C_2V_0]-n_fk_fV_0^{n_f-1}M_1^{-1}\int_0^L\frac{A_d}{\Delta^{n_f}}\eta(\xi)\eta^T(\xi)\,d\xi$$

$$A_{36}=O_{N_x}\times O_{N_t}$$

$$A_4=[A_{41}\ \ A_{42}\ A_{43}\ \ A_{44}\ \ A_{45}\ \ A_{46}]$$

$$A_{41}=-\frac{n}{2}a^2\epsilon M_2^{-1}\psi(L)+\frac{\rho na\epsilon\zeta}{M}M_2^{-1}\left[\int_0^L J\psi(\xi)\varphi_S'(\xi)d\xi\right]$$

$$A_{42}\ =-\frac{n}{2}a^2\epsilon M_2^{-1}\psi(L)\eta^T(L)+\frac{\rho na\epsilon\zeta}{M}M_2^{-1}\left[\int_0^L J\psi(\xi)\varphi_S'(\xi)d\xi\right]\eta^T(L)$$

$$A_{43}=-M_2^{-1}[K_4+V_0^2K_5]+\frac{n}{2}a^2\epsilon\frac{V_0}{\Omega}M_2^{-1}\psi(L)\psi^T(L)-\frac{\rho na\epsilon\zeta}{M}\frac{V_0}{\Omega}M_2^{-1}\left[\int_0^L J\psi(\xi)\varphi_S'(\xi)d\xi\right]\psi^T(L)$$

$$A_{44}=-2\rho V_0M_2^{-1}\int_0^L J\psi(\xi)\varphi_S^{"}(\xi)d\xi$$

$$A_{45}=O_{N_X}\times O_{N_t}$$

$$A_{46}=-M_2^{-1}[C_3+2C_4V_0]-\frac{1}{2}a^2\sigma\gamma lM_2^{-1}\psi(L)\psi^T(L)\frac{\partial\mu}{\partial\omega}|_{\omega=\Omega}\ -n_fk_f\Omega^{n_f-1}M_2^{-1}\int_0^L\frac{r_d^{n_f+1}A_d}{\Delta^{n_f}}\psi(\xi)\psi^T(\xi)\,d\xi$$

$$B_1=O_{N\times N}$$

$$B_2=\frac{na\epsilon\zeta}{M}\begin{bmatrix}1 & \eta^T(L) & -\frac{V_0}{\Omega}\psi^T(L)\end{bmatrix}$$

$$B_3=[B_{31}\quad B_{32}\quad B_{33}]$$

$$B_{31}=na\epsilon\zeta M_1^{-1}\eta(L)-\frac{\rho na\epsilon\zeta}{M}M_1^{-1}\left[\int_0^L A\eta(\xi)\big(1+U_s'(\xi)\big)\,d\xi\right]$$

$$B_{32} = na\epsilon\zeta M_1^{-1}\eta(L)\eta^T(L) - \frac{\rho na\epsilon\zeta}{M} M_1^{-1}\left[\int_0^L A\eta(\xi)\left(1 + U_s'(\xi)\right) d\xi\right] \eta^T(L)$$

$$B_{33} = -na\epsilon\zeta \frac{V_0}{\Omega} M_1^{-1}\eta(L)\psi^T(L) + \frac{\rho na\epsilon\zeta}{M}\frac{V_0}{\Omega} M_1^{-1}\left[\int_0^L A\eta(\xi)\left(1 + U_s'(\xi)\right) d\xi\right]\psi^T(L)$$

$$B_4 = [B_{41} \quad B_{42} \quad B_{43}]$$

$$B_{41} = \frac{n}{2}a^2\epsilon M_2^{-1}\psi(L) - \frac{\rho na\epsilon\zeta}{M} M_2^{-1}\left[\int_0^L J\psi(\xi)\varphi_S'(\xi)d\xi\right]$$

$$B_{42} = \frac{n}{2}a^2\epsilon M_2^{-1}\psi(L)\eta^T(L) - \frac{\rho na\epsilon\zeta}{M} M_2^{-1}\left[\int_0^L J\psi(\xi)\varphi_S'(\xi)d\xi\right]\eta^T(L)$$

$$B_{43} = -\frac{n}{2}a^2\epsilon\frac{V_0}{\Omega} M_2^{-1}\psi(L)\psi^T(L) + \frac{\rho na\epsilon\zeta}{M}\frac{V_0}{\Omega} M_2^{-1}\left[\int_0^L J\psi(\xi)\varphi_S'(\xi)d\xi\right]\psi^T(L)$$